The Astrophysical Journal, 740:99 (10pp), 2011 October 20 doi:10.1088/0004-637X/740/2/99

THE STARBURST–ACTIVE-GALACTIC-NUCLEUS CONNECTION: A *SPITZER* SEARCH FOR ACTIVE GALACTIC NUCLEI IN INFRARED-SELECTED STARBURST GALAXIES

T. G. Dixon and R. D. Joseph
Institute for Astronomy, University of Hawaii, 2680 Woodlawn Drive, Honolulu, HI 96822, USA; dixon@ifa.hawaii.edu, joseph@ifa.hawaii.edu
Received 2010 November 19; accepted 2011 July 25; published 2011 October 4

ABSTRACT

We present observations of a sample of 28 luminous infrared galaxies (LIRGs) from the *IRAS* Bright Galaxy Catalog. These galaxies were previously observed by Goldader et al. using 2 μm spectroscopy on UKIRT. They found that stellar population synthesis models constrained by the spectroscopic diagnostics implied star formation rates that accounted for their infrared luminosities, and there was also no spectroscopic evidence for "buried" active galactic nuclei (AGNs) at 2 μm. To search for evidence of AGNs buried deeply in extinction we have supplemented the UKIRT spectra with *Spitzer* mid-infrared (5.2–38.0 μm) spectra. Using a variety of spectroscopic diagnostics we find that ∼50% of the sample shows some evidence for an AGN. We also find that the luminosity of about ∼(17 ± 4)% of our sample is probably dominated by emission from AGNs, and the remaining ∼(80 ± 4)% have luminosities dominated by starbursts. Since ∼50% of the sample shows some evidence of concurrent AGN and starburst activities this suggests that both AGNs and starbursts commonly coexist in the LIRGs' phase of evolution. The sample consists of galaxies that show no AGN signatures at wavelengths less than 2 μm, so it appears that at wavelengths below 2 μm extinction in these galaxies masks the detection of AGNs in these and other LIRGs.

Key words: galaxies: active – galaxies: evolution – galaxies: interactions – galaxies: starburst

1. INTRODUCTION

Since the discovery of a large population of luminous infrared galaxies (LIRGs; $10^{11} L_{\rm sun} \geqslant L_{(8-1000)\,\mu{\rm m}} < 10^{12} L_{\rm sun}$) (e.g., Rieke & Low 1972) there has been controversy concerning the energy sources that power these galaxies. Both AGNs and recent bursts of star formation ("starbursts") were proposed as the underlying energy sources powering these galaxies, and this has become known as the "Starbursts–Monsters" Controversy (Heckman et al. 1983). This controversy has reached its apotheosis in attempts to understand the more luminous ULIRGs ($L_{(8-1000)\,\mu{\rm m}} \geqslant 10^{12} L_{\rm sun}$), but that is not the subject of this paper. Both AGNs and starbursts are widely acknowledged to exist deeply buried in interstellar dust, and the extinction problem has made it difficult to reach an incontrovertible conclusion. In particular, those who have favored AGNs but failed to find the diagnostics indicative of AGN activity have argued that there must be too much extinction to see evidence of an AGN at optical or near-infrared wavelengths (e.g., Sanders 1999), whereas those favoring starbursts have argued that in the majority of cases all the diagnostic evidence available indicates that recent star formation accounts for the bolometric luminosity (e.g., Joseph 1999).

Most LIRGs are recognized to have morphological features, such as tidal bridges and tails, characteristic of interacting or merging galaxies (Toomre & Toomre 1972). Joseph et al. (1984), Joseph & Wright (1985), Wright et al. (1988), and others have shown that interactions and mergers of spiral galaxies are effective triggers of starbursts. In fact, Larson & Tinsley (1978) compared the *UVB* colors of galaxies in Arp's peculiar galaxy catalog to those of a control sample, and showed that the greater dispersion in the colors of the interacting galaxies could be understood as the result of recent star formation triggered by interactions.

Evidence has been accumulating that starburst activity is sometimes present in the central regions of Seyfert 2 galaxies. A number of optical studies have revealed evidence for starburst activity in a (generally minor) fraction of Seyfert 2 galaxies (Rodriguez Espinosa et al. 1987; Shier et al. 1996; Heckman et al. 1983; Cid Fernandes et al. 2001; Storchi-Bergmann et al. 2001). In fact, the prototypical Seyfert 2 galaxy NGC 1068 is an excellent example. Sani et al. (2010) have found evidence for intense ongoing star formation in a sample of narrow-line Seyfert 1 galaxies. These results suggest that there may be a connection between starburst and AGN activities.

This idea has gained strong support from modeling of interactions and mergers. Numerical simulations of gas-rich spiral galaxy mergers that have included gas dynamics have supported the notion that major mergers between gas-rich spirals do lead to rapid star formation (Noguchi 1988; Barnes & Hernquist 1991, 1992; Schweizer 2005). Mihos & Hernquist (1996) and Hopkins et al. (2010) have done high-resolution hydrodynamic simulations for the formation of starbursts and AGNs in mergers, and then modeled the relative contributions of "normal" galaxy disks, merger-induced starbursts, and merger-induced AGNs to predict the contributions of all three to the total infrared luminosities of galaxies as they evolve from high to low redshift. Their results indicate that, while merger-induced star formation dominates the merger-induced AGN contribution to the infrared luminosity, both processes should be present in mergers for at least a fraction of the merger evolution timescale.

Goldader et al. (1997) identified a subset of a complete sample of LIRGs selected from the *IRAS* Bright Galaxy Catalog (Soifer et al. 1987), which is a statistically complete sample of 324 galaxies visible from the northern hemisphere at galactic latitudes of 30° or larger. Goldader et al. limited their sample to 97 systems (several objects were clearly interacting) with $L_{\rm IR} \geqslant 10^{11.2} L_{\rm sun}$, declination between −40° and +60° that could be observed with the UKIRT telescope. Of these 97 systems, Goldader et al. (1997) observed 43 systems using *K*-band spectroscopy on the UKIRT. Goldader et al. (1997) showed that starburst models were consistent with the *K*-band fluxes and that star formation accounted for the total infrared luminosities of the sample. Moreover, there was no evidence of AGN activity in the *K*-band that had not previously been observed in the optical spectra of these galaxies. However, the

Table 1
Observed LIRG Sample Properties

ID[a]	Name	R.A.[b]	Decl.	cz[c] (km s^{-1})	Distance (Mpc)	FIR Luminosity $\log(L_{\rm FIR}/L_{\rm sun})$
1	MCG−03-04-014	$1^{h}5^{m}42^{s}$	$-17^\circ7'1''$	10040	131.0	11.58
2	IR01364−1042	$1^{h}36^{m}24^{s}$	$-10^\circ42'25''$	14250	187.2	11.76
3	NGC695	$1^{h}48^{m}28\overset{s}{.}1$	$22^\circ20'10''$	9769	129.8	11.64
4	IR03359+1523	$3^{h}35^{m}57\overset{s}{.}1$	$15^\circ23'6''$	10600	140.1	11.47
5	UGC3094	$4^{h}32^{m}38\overset{s}{.}3$	$19^\circ4'7''$	7407	98.1	11.36
6	NGC2342	$7^{h}6^{m}20\overset{s}{.}5$	$20^\circ43'4''$	5256	71.0	11.22
7	NGC2388	$7^{h}25^{m}38\overset{s}{.}2$	$33^\circ55'20''$	4060	56.4	11.18
8	MCG+08-18-012	$9^{h}33^{m}18\overset{s}{.}5$	$48^\circ41'53''$	7790	107.7	11.31
9	NGC3110	$10^{h}1^{m}32\overset{s}{.}2$	$-6^\circ14'2''$	4840	66.0	11.22
10	IR10173−0828	$10^{h}17^{m}22\overset{s}{.}1$	$8^\circ28'41''$	14390	193.7	11.77
11	MCG−00-29-023	$11^{h}18^{m}38\overset{s}{.}6$	$-2^\circ42'36''$	7230	98.6	11.23
12	UGC6436	$11^{h}23^{m}9\overset{s}{.}8$	$14^\circ56'53''$	10216	139.4	11.52
13	Arp193	$13^{h}18^{m}19^{s}$	$34^\circ23'49''$	6870	96.8	11.58
14	MRK1490	$14^{h}17^{m}53\overset{s}{.}76$	$49^\circ27'55\overset{''}{.}7$	7696	108.0	11.32
15	Arp302	$14^{h}54^{m}47\overset{s}{.}8$	$24^\circ48'58''$	10100	139.7	11.65
16	IZw107N	$15^{h}16^{m}19^{s}$	$42^\circ55'41''$	12043	166.0	11.85
17	NGC6090	$16^{h}10^{m}24^{s}$	$52^\circ35'6''$	8733	122.0	11.49
18	IR16164−0746	$16^{h}16^{m}29\overset{s}{.}5$	$-7^\circ46'49''$	6857	94.8	11.43
19	NGC6285	$16^{h}57^{m}44\overset{s}{.}9$	$59^\circ0'40''$	5600	80.4	11.33
20	NGC6286	$16^{h}57^{m}44\overset{s}{.}9$	$59^\circ0'40''$	5600	80.4	11.33
21	IR17132−5313	$17^{h}13^{m}14\overset{s}{.}2$	$53^\circ13'52''$	15212	208.0	11.88
22	IR17138−1017	$17^{h}13^{m}50\overset{s}{.}7$	$-10^\circ17'29''$	5261	73.1	11.39
23	Zw448.020	$20^{h}55^{m}5\overset{s}{.}3$	$16^\circ56'3''$	10900	147.4	11.89
24	ESO602-G025	$22^{h}28^{m}42\overset{s}{.}7$	$-19^\circ17'31''$	7263	95.5	11.25
25	UGC12150	$22^{h}38^{m}53\overset{s}{.}6$	$33^\circ59'12''$	6413	87.6	11.29
26	Zw453.062	$23^{h}2^{m}28\overset{s}{.}1$	$19^\circ16'55''$	7373	99.1	11.28
27	MCG+07-23-019	$11^{h}1^{m}5\overset{s}{.}04$	$41^\circ7'7\overset{''}{.}6$	10810	145.0	11.61
28	CGCG052-037	$16^{h}28^{m}27\overset{s}{.}22$	$4^\circ11'23\overset{''}{.}2$	7342	103.0	11.38

Notes.
[a] Column 1 is the galaxy ID.
[b] R.A. and Decl. in B1950.
[c] Columns 5–7 are from Goldader et al. (1997).

question has remained whether extinction was still a significant factor even at 2 μm. We have therefore used the *Spitzer* Infrared Spectrograph (IRS) mid-infrared spectrometer to obtain mid-infrared diagnostics for 28 LIRGs from the Goldader et al. (1997) sample. These 28 LIRGs showed no AGN signatures in optical or near-infrared. The primary aim was to search for AGN features in the mid-infrared (5–35 μm), which would be even less subject to extinction than 2 μm spectra, in order to investigate the putative connection between starbursts and AGNs in powering LIRGs. We also hoped to be able to estimate the contribution of AGNs to the $L_{\rm FIR}$ of the sample. We note that our sample of 28 galaxies will include only AGNs that are too deeply buried in extinction to be detected in either the optical or the *K*-band. Thus, there may be differences between the results for our sample and samples that include optically classified AGNs. Throughout this paper we adopt the cosmology $H_0 = 75$ km s^{-1} Mpc^{-1} and $q_0 = 0$

After this manuscript was submitted we learned that Petric et al. (2011) had a similar study of LIRGs in press. In Section 6 we compare our results with those found by Petric et al.

2. OBSERVATIONS

This paper is based on *Spitzer* (Werner et al. 2004) IRS observations of 28 LIRG galaxies from the *IRAS* Bright Galaxy Samples of Soifer et al. (1987), listed in Table 1. The *Spitzer* IRS (Houck et al. 2004) provides unprecedented mid-infrared sensitivity for low- and moderate-resolution spectroscopy from 5.2 to 38.0 μm. IRS is composed of four separate modules, with two modules providing a spectral resolution $R \sim 60$–120 over 5.2–38.0 μm and two modules providing a spectral resolution $R \sim 600$ over 9.9–37.2 μm. For the work herein we used three of the four *Spitzer* modules; the long-wavelength low-resolution module (LL) was not used. For target acquisition the "no peak-up" option was used. The data were processed through the Spitzer Science Center's IRS pipeline data reduction software. This performs standard data reduction tasks such as dark current subtraction. We used the IRSClean application to correct for hot or bad pixels.

3. DIAGNOSTIC TOOLS

Mid-infrared spectroscopy provides a variety of diagnostics of both starburst and AGN activities, as previously done by Veilleux et al. (2009), Genzel et al. (1998), Sturm et al. (2002), and others. The ion [Ne V] has an ionization potential of 97 eV and so the coronal lines at 14.3 μm and 24.3 μm are good indicators of the presence of an AGN (Spinoglio & Malkan 1992). Conversely, the Ne II line is strong in the H II regions of starburst galaxies but is generally weak in AGNs. Thus the line ratios [Ne V]14.3 μm/[Ne II]12.8 μm and [Ne V]24.3 μm/[Ne II]12.8 μm can be used to identity galaxies that contain AGNs (Genzel et al. 1998). Sturm et al. (2002) have measured the above lines using *ISO*-SWS for a sample of 29 AGN galaxies. For their AGN sample the [Ne v]14.3 μm/[Ne ii]12.8 μm and [Ne v]24.3 μm/[Ne ii] 12.8 μm line ratios have median values of 0.45 and 0.35, respectively. The same line ratios in starburst galaxies that do not contain any AGN have values that are one or two orders lower in magnitude (Genzel et al. 1998).

A strong [O iv] 25.9 μm line is often detected in LIRGs. The [O iv] ion has a lower ionization potential of 55 eV and can be weakly produced in starburst galaxies by supernovae and strong wind shocks. Nevertheless, while strong [O iv] lines are found in AGNs they are never strong when observed in starburst galaxies (Sturm et al. 2002), making a strong [O iv]25.9 μm/ [Ne ii]12.8 μm ratio a good diagnostic for the presence of an AGN. For the Sturm et al. (2002) sample of AGNs, the [O iv]25.9 μm/[Ne ii]12.8 μm ratio has a median value of about 1. In the galaxy templates used by Genzel et al. (1998), the [O iv]25.9 μm/[Ne ii]12.8 μm is typically one to two orders of magnitude lower in starburst galaxies than in AGN galaxies.

The [Ne iii]15.6 μm/[Ne ii]12.8 μm ratio can be used to determine the temperature of an emitting region. In the case of starburst galaxies this ratio is typically 0.1 or lower (Ho & Keto 2007), while in galaxies that host an AGN this ratio is expected to be about 1 or larger. The AGN galaxies of Sturm et al. (2002) have a median [Ne iii]15.6 μm/[Ne ii]12.8 μm of 1.1 and we use this value to indicate the presence of an AGN in our sample.

PAH (Polycyclic Aromatic Hydrocarbon) emission features are extremely strong in starburst galaxies but are weak or absent in AGNs (Roche et al. 1991; Tielens et al. 2004). We use the strength of the PAH 7.7 μm feature as described by Lutz et al. (1998) to indicate the presence or absence of an AGN. The PAH 7.7 μm strength is determined by measuring the peak at 7.7 μm and subtracting the continuum value at 7.7 μm. The continuum at 7.7 μm is determined by linearly interpolating between the continuum point at 5.9 μm and the continuum point at 10.9 μm. Lutz et al. (1998) suggest that a PAH 7.7 μm strength <1 is a good indicator of an AGN. In the starburst templates of Genzel et al. (1998), the median PAH 7.7 μm strength is 3.1, while the median PAH 7.7 μm for their AGN templates is 2.4. As well as using the PAH 7.7 μm feature as a diagnostic in its own right, we also use the [O iv]25.9 μm/[Ne ii]12.8 μm versus the PAH 7.7 μm strength with the Genzel et al. (1998) calibration curve to measure the contribution of an AGN to each galaxy's $L_{\rm FIR}$.

AGNs produce a warm dust component in the mid-infrared and the strength of continuum flux ratios such as the $IRAS_{5.9\,\mu\rm m}$ to $IRAS_{60\,\mu\rm m}$, $IRAS_{25\,\mu\rm m}$ to $IRAS_{60\,\mu\rm m}$, and $f_{30\,\mu\rm m}$ to $f_{15\,\mu\rm m}$ (Lutz et al. 1998; Farrah et al. 2007; Veilleux et al. 2009) have been found to correlate with the presence of AGNs. We use the continuum ratio $\log(\frac{f_{30}}{f_{15}})$ to measure the strength of the warm dust component in each galaxy. Veilleux et al. (2009) find that starburst galaxies have $\log(\frac{f_{30}}{f_{15}}) = 1.55$ while AGNs have $\log(\frac{f_{30}}{f_{15}}) = 0.2$.

In the mid-infrared, the spectral energy distribution of an AGN is well fitted by a power law. Conversely, the mid-infrared spectra of starburst galaxies have strong PAH 7.7 μm emission and strong 10 μm silicon absorption features that readily distinguish these from a simple power-law spectral shape. One caveat however is that the power-law fit is most appropriate for QSOs or Seyfert 1 AGNs. Seyfert 2 AGNs still have moderate PAH 7.7 μm emission and 10 μm silicon absorption features, though these are weaker than in starburst galaxies (Veilleux et al. 2009). We use the 7–14 μm portion of our low-resolution spectra and fit a line to the $\log(f_v)$ versus $\log(\lambda)$ to determine the spectral index and goodness of fit for a power law for each galaxy.

In summary, we use seven basic diagnostics. We use four MIR line ratios: (1) [Ne iii]15.6 μm/[Ne ii]12.8 μm, (2) [Ne v]14.3 μm/[Ne ii]12.8 μm, (3) [Ne v]24.3 μm/[Ne ii] 12.8 μm, and (4) [O iv]25.9 μm/[Ne ii]12.8 μm. We use two continuum diagnostics: (1) a fit to the MIR spectral-slope and (2) the $\log(\frac{f_{30}}{f_{15}})$ ratio. We also use the strength of the PAH 7.7 μm feature. An eighth diagnostic that is somewhat more sophisticated is produced by combining the PAH 7.7 μm strength with the [O iv]25.9 μm/[Ne ii]12.8 μm ratio. Using the calibration curve of Genzel et al. (1998) this eighth diagnostic can be used to estimate the contribution of an AGN to each galaxy's luminosity.

4. DATA ANALYSIS

4.1. Line Ratios and PAH Features

Table 2 shows the observed values of the line ratios [Ne v]14.3 μm/[Ne ii]12.8 μm, [Ne v]24.3 μm/[Ne ii]12.8 μm, and [O iv]25.9 μm/[Ne ii]12.8 μm. These ratios are also shown in Figure 1 and are derived from the spectral line fluxes in Table 3. We have linearly interpolated between the AGN and starburst values of these line ratios to get an estimate of the AGN contribution to each galaxy's $L_{\rm FIR}$. Five galaxies (18% of the sample) have [Ne v]14.3 μm/[Ne ii]12.8 μm, [Ne v]24.3 μm/ [Ne ii]12.8 μm, or [O iv]25.9 μm/[Ne ii]12.8 μm values that are more than 50% of the median value found in AGNs by Sturm et al. (2002). Thus, the power output of these may be dominated by the power output of their AGNs. Additionally, three galaxies (11% of the sample) have line ratios of more than 25% of the median value seen in AGNs, suggesting that these galaxies may also have some AGN contribution to their power output.

The Ne ii line is detected in all galaxies except Arp302 and the Ne iii line is detected in all galaxies except galaxies MCG+08-18-012, IR10173−0828 and Arp302. Table 4 shows the measured [Ne iii]15.6 μm/[Ne ii]12.8 μm values. Two galaxies (Zw 448.020, MCG+07-23-019, 7% of the sample) have [Ne iii]15.6 μm/[Ne ii]12.8 μm ratios >1, which indicates that these galaxies have strong contributions to their luminosity from AGNs.

The PAH 7.7 μm strengths given in Table 3 and plotted in Figure 2 show that six galaxies (21%) have PAH strengths of <1 which suggests that AGNs make a significant contribution to the luminosity of these galaxies. Additionally, five galaxies (18%) have PAH 7.7 μm strengths <2.1 (which is the average PAH strength found in the AGN sample of Genzel et al. 1998); consequently, these galaxies may also have AGNs contributing to their luminosity.

Figure 3 shows the measured [O iv]25.9 μm/[Ne ii]12.8 μm line ratios, the PAH 7.7 μm strengths, and the calibration curve of Genzel et al. (1998). This curve has been used to estimate quantitatively the contribution of an AGN to each galaxy's power output. Three galaxies (11%) in our sample have the low PAH 7.7 μm strengths and high [O iv]25.9 μm/[Ne ii]12.8 μm ratios characteristic of galaxies dominated by AGNs. An additional 12 galaxies (43%) of our sample have locations on the Genzel curve that suggest they have from 5% to 50% of their luminosity provided by an AGN. Using the Genzel curve the

Table 2
Coronal Diagnostic Line Ratios and a Rough Estimate of Percentage AGN Contribution

Name	$\frac{[\mathrm{Ne\,V}]24.3\,\mu\mathrm{m}}{[\mathrm{Ne\,II}]12.8\,\mu\mathrm{m}}$	Error	AGN (%)	$\frac{[\mathrm{Ne\,V}]14.3}{[\mathrm{Ne\,II}]12.8\,\mu\mathrm{m}}$	Error	AGN (%)	$\frac{[\mathrm{O\,IV}]25.9\,\mu\mathrm{m}}{[\mathrm{Ne\,II}]12.8\,\mu\mathrm{m}}$	Error	AGN (%)
MCG−03-04-014	0.117	0.010	39	0.025	0.003	6	0.097	0.005	10
IR01364−1042							0.502	0.036	50
NGC695	0.009	0.005	3				0.017	0.005	2
IR03359+1523	0.016	0.006	5						
UGC3094				0.077	0.005	19	0.260	0.007	26
GC2342				0.032	0.005	8	0.020	0.006	2
NGC2388				0.056	0.003	14	0.033	0.004	3
MCG+08-18-012							0.480	0.202	48
NGC3110	0.006	0.004	2	0.013	0.003	3	0.012	0.003	1
IR10173−0828	0.326	0.059	109				0.505	0.092	50
MCG−00-29-023									
UGC6436									
Arp193	0.010	0.003	3	0.009	0.002	2	0.067	0.003	7
MRK1490				0.014	0.003	3			
Arp302									
IZw107N							0.034	0.014	3
NGC6090									
IR16164−0746				0.019	0.002		0.144	0.005	15
NGC6285									
IR17132−5313							0.072	0.004	13
IR17132−5313									
IR17138−1017	0.017	0.004	6	0.034	0.005	8			
Zw448.020	0.107	0.047	36	0.391	0.021	98	0.089	0.048	9
ESO602-G025	0.062	0.007	20	0.041	0.004	10	0.158	0.007	16
UGC12150				0.057	0.012	14			
Zw453.062	0.107	0.007	36	0.181	0.005	45	0.244	0.008	24
MCG+07-23-019	0.230	0.085	77	0.332	0.028	83			
cgcg052-037	0.008	0.003	3	0.018	0.002	5			

Note. Rough percentage AGN contributions are estimated by linearly interpolating between the median AGN and starburst line ratios given in Sturm et al. (2002).

total L_{FIR} contribution of AGNs to the L_{FIR} of our sample is (17 ± 4)%.

4.2. Mid-infrared Spectral Energy Distributions

In the 7–14 μm range, six galaxies (21%) have mid-infrared spectra that are well fitted by a power law of the form $F_\nu \propto \lambda^{-\alpha}$. This power-law shape is characteristic of AGN spectral energy distributions and suggests that AGNs may be dominating the output of these galaxies. The remaining 22 galaxies in the sample are not well fitted by a power law and show strong PAH 7.7 μm and strong 10 μm silicon absorption features, suggesting that these galaxies are dominated by energy produced in starburst regions. The power-law spectral indices and uncertainties for these six galaxies are shown in Table 5 while Figure 4 shows the best-fit spectral indices for all of the LIRG sample. Those that have obvious power-law shapes rather than starburst-like shapes (i.e., with strong broad PAH 7.7 μm emission and 10 μm silicon absorption features) have significantly larger spectral indices (typically $\alpha > 3$). Figure 5 shows, in the upper panel, the six AGN-like spectra (normalized to have an area of 1.0 under the curve). The middle panel in this figure shows a similar plot for the normalized spectra of the starburst-like galaxies in our sample. In the same figure the bottom panel shows a plot of the average of the six AGN-like normalized spectra and the average of the starburst-like spectra. The averaged spectra in Figure 5 have very different spectral slope and a different structure in the mid-infrared.

The starburst-averaged spectrum has a strong PAH 7.7 μm feature and a strong 10μm silicon absorption feature, while in the AGN-averaged spectrum these features are weak or absent and the spectrum has a power-law shape. PAH features are usually observed to be prominent in starburst galaxies, and a good correlation between the strength of PAH features and IR luminosity has been demonstrated for starburst galaxies by Brandl et al. (2006). However, PAH features are generally weak or absent in AGNs (Weedman et al. 2005), but the nature of PAH features and their use as indicators of star formation is still poorly understood (Peeters et al. 2004). The absence of PAH features in AGNs is thought to be due to a combination of two factors. First, AGNs have a harder radiation field than is found in starburst galaxies. This is generated by the AGN's accretion disk and is thought to destroy the PAHs. Second, in a luminous AGN the mid-infrared continuum is extremely strong and can wash out the PAH features even if there is a high rate of star formation (Laurent et al. 2000). This power-law spectral shape in the mid-infrared is a fast and efficient way of selecting galaxies that are candidates for AGN-dominated galaxies. We note that all but one of the galaxies (Arp302) that have an AGN power-law-like spectral shape also have [Ne V]24.3 μm/[Ne II]12.8 μm, [Ne V]14.3 μm/[Ne II]12.8 μm, or [O IV]25.9 μm/[Ne II]12.8 μm values and PAH 7.7 μm strengths that suggest a significant AGN contribution to their luminosity. In the case of Arp302 we detect no high-ionization lines. However, Arp302 does have a weak PAH strength and weak [Ne II] and [S III] lines which are also characteristics of AGNs.

Table 3

The Fluxes Measured for Each Galaxy in Units of 10^{-14}(erg cm^{-2} s^{-1}). Also Shown are the Star Formation Rates Based on the Luminosity of ([Ne II]+[Ne III]) and the PAH Strengths

Galaxy	[Ne V] 14.3 μm	Error	[Ne V] 24.3 μm	Error	[O IV] 25.9 μm	Error	[Ne II] 12.8 μm	Error	[Ne III] 15.55 μm	Error	[S III] 18.7 μm	Error	[S III] 33.48 μm	Error	Star[a] Formation Rate (Msun yr^{-1})	Error (Msun yr^{-1})	PAH[b] Strength 7.7 μm	Error	AGN[c] (%)	f_{30} Janskys	f_{15} Janskys	$\log(\frac{f_{30}}{f_{15}})$	Error	AGN[d] (%)
MCG−03-04-014	2.36	0.29	10.86	0.94	8.99	0.49	92.85	0.46	13.66	0.36	47.85	1.3	96.89	1.02	135	3.4	5.56	0.07	0	2.37	0.28	0.93	0.012	46
IR01364−1042					8.08	0.43	16.13	0.78	3.35	0.28	1.54	0.3	20.31	0.84	47	4.6	1.36	0.04	74	1.68	0.13	1.11	0.007	32
NGC695			0.66	0.37	1.29	0.35	74.88	0.4	12.53	0.31	29.32	0.88	63.11	1.24	102	2.6	2.34	0.02	4	1.57	0.25	0.8	0.015	56
IR03359+1523			0.85	0.3			52.01	0.83	16.04	0.24	24.31	0.3	19.55	0.92	84	2	0.37	0	100	1.36	0.3	0.66	0.029	66
UGC3094	3.75	0.23			12.68	0.32	48.82	0.48	18.84	0.26	78.52	2.75	69.7	0.88	45	0.8	1.12	0.01	91	1.68	0.26	0.81	0.02	55
NGC2342	1.49	0.25			0.92	0.27	46.8	0.32	7.42	0.24	16.1	2.52	36.94	0.99	19	0.6	2.29	0.04	8	1.36	0.14	0.99	0.008	42
NGC2388	6.72	0.41			3.94	0.54	120.93	0.5	12.94	0.36	61.98	3.51	39.44	1.54	30	0.8	1.95	0.02	32	5.31	0.41	1.11	0.006	32
MCG+08-18-012					0.44	0.18	0.92	0.12					3.61	0.58	1	0	0.44	0.01	100	0.12	0.03	0.6	0.024	70
NGC3110	1.17	0.26	0.5	0.32	1.09	0.32	91.39	0.39	10.94	0.23	62.1	2.85	68.48	1.08	31	0.7	2.77	0.03	0	1.69	0.18	0.97	0.006	43
IR10173−0828			0.98	0.17	1.51	0.27	2.99	0.11					4.16	0.57	8	0	0.33	0.01	100	1.69	0.21	0.91	0.01	48
MCG−00-29-023							40.4	0.57	8.03	0.34	13.31	0.67	42.59	0.83	33	1.4	1.59	0.02	58	2.12	0.34	0.79	0.015	56
UGC6436							29.8	0.23	3.13	0.22	9.85	0.52	20.78	0.72	44	3.1	3.83	0.07	0	1.31	0.16	0.91	0.014	47
Arp193	1.2	0.22	1.44	0.45	9.38	0.47	138.81	0.42	25.9	0.26	34.05	0.47	113.53	1.95	107	1.1	3.94	0.08	0	4.71	0.22	1.33	0.002	16
MRK1490	0.72	0.18					52.83	0.41	5.18	0.21	20.94	1.68	17.49	1.23	47	1.9	4.12	0.07	0	2.12	0.2	1.03	0.005	39
Arp302											3.48	0.46	3.58	0.68	11	0	0.94	0.04	100	0.12	0.04	0.48	0.096	79
IZw107N					0.67	0.28	19.9	0.74	4.81	0.38	6.81	0.36	10.49	0.83	47	4.1	3.1	0.16	0	0.75	0.08	0.97	0.01	43
NGC6090							95.92	0.56	26.15	0.31	47.86	7.76	94.23	0.92	126	1.7	2.5	0.02	0	2.2	0.24	0.96	0.008	44
IR16164−0746	1.29	0.17			10.03	0.31	69.36	0.34	24.32	0.2	10.96	0.31	44.73	1.01	58	0.6	3.66	0.08	0	2.85	0.15	1.28	0.004	20
NGC6285							28.16	0.32	4.31	0.19	20.48	1.91	32.37	6.4	15	0.7	5.24	0.17	0	0.49	0.04	1.09	0.01	34
IR17132−5313					3.59	0.18	50.06	1.12	6.77	0.21	12.09	1.63	44.86	7.98	26	1	4.63	0.08	0	1	0.09	1.05	0.012	37
IR17132−5313							50.26	0.13	5.63	0.19	17.9	0.32	49.11	1.05	168	5.7	6.68	0.08	0	1.65	0.16	1.01	0.007	40
IR17138−1017	4.41	0.6	2.2	0.48			130.05	0.68	24.42	0.47	44.68	3.42	114.07	1.63	57	1.1	4.73	0.03	0	3.75	0.31	1.08	0.007	35
Zw448.020	2.7	0.12	0.74	0.33	0.61	0.33	6.91	0.22	4.02	0.15	9.36	0.55	24.22	0.98	16	0.8	0.01	0	100	0.91	0.12	0.88	0.002	50
ESO602-G025	2.26	0.23	3.41	0.37	8.77	0.38	55.52	0.39	13.04	0.21	17.27	2.02	39.79	1.25	43	0.8	2.24	0.03	11	2.11	0.27	0.89	0.014	49
UGC12150	1.41	0.29					25.02	0.43	6.79	0.28	14.57	2.62	48.66	1.5	17	0.8	2.72	0.04	0	2.5	0.17	1.17	0.003	28
Zw453.062	5.25	0.14	3.12	0.21	7.11	0.21	29.08	0.26	13.97	0.15	11.48	1.19	23.74	0.85	29	0.4	2.31	0.04	6	1.83	0.14	1.12	0.007	32
MCG+07-23-019	0.9	0.07	0.62	0.23			2.71	0.08	2.12	0.09	8.95	0.5	33.25	1.09	7	0.4	0.51	0.01	100	1.29	0.11	1.07	0.006	36
cgcg052-037	1.67	0.18	0.76	0.32			91.21	0.41	8.43	0.2	31.78	0.44	65.36	0.91	73	1.8	2.66	0.04	0	2.24	0.23	0.99	0.006	42

Notes.

[a] Determined from the ($L_{[\mathrm{Ne\,II}]12.8\,\mu\mathrm{m}} + L_{[\mathrm{Ne\,III}]15.6\,\mu\mathrm{m}}$) and the calibration of Ho & Keto (2007).

[b] PAH 7.7 μm strength as defined by Lutz et al. (1998).

[c] Estimate of the percentage AGN contribution to luminosity using PAH 7.7 μm with linear interpolation between starburst = 2.4 and AGN = 1.

[d] Estimate of the percentage AGN contribution to luminosity using $\log(\frac{f_{30}}{f_{15}})$ with linear interpolation between starburst = 1.55 and AGN = 0.2.

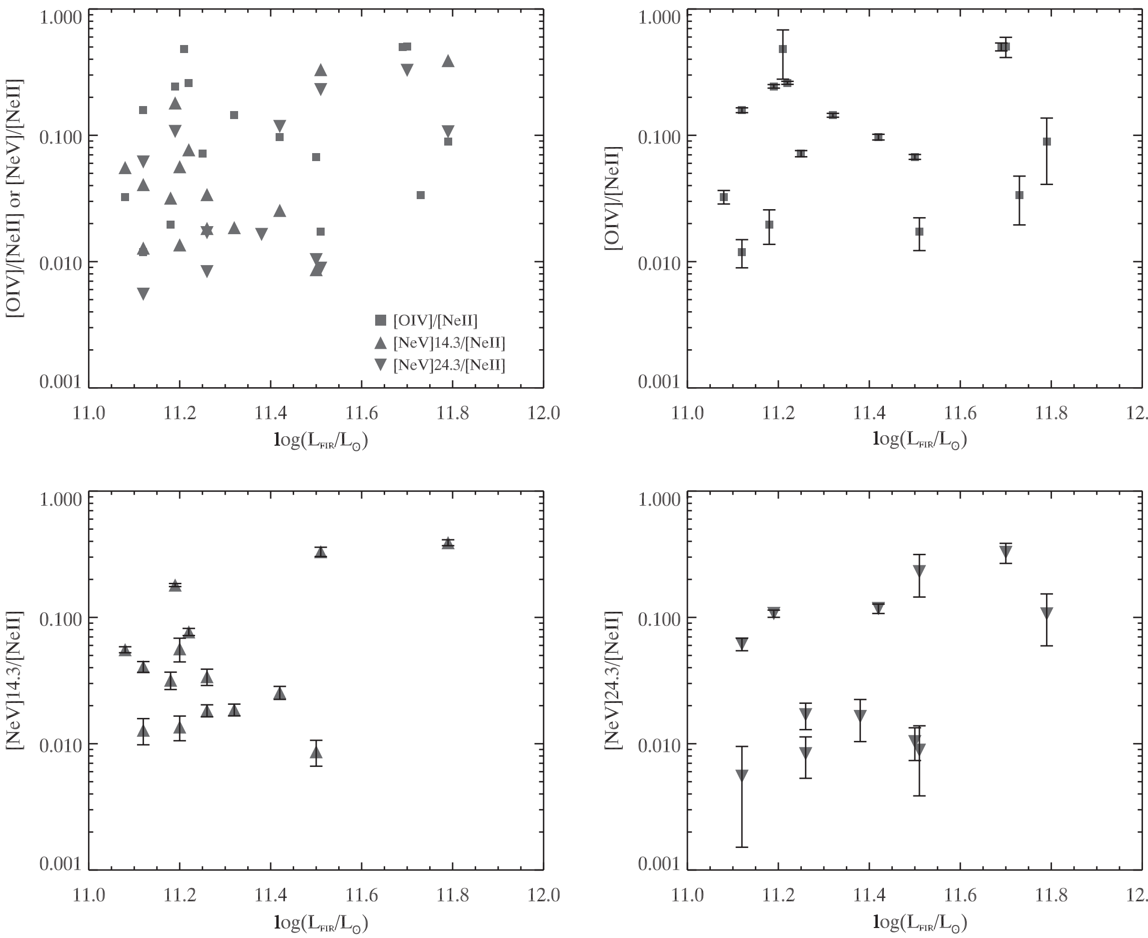

Figure 1. [O IV]25.9 μm/[Ne II]12.8 μm, [Ne V]14.3 μm/[Ne II]12.8 μm, and [Ne V]24.3 μm/[Ne II]12.8 μm ratios from our sample of galaxies vs. each galaxy's FIR luminosity. The first panel shows a summary of all the data in the three following panels.

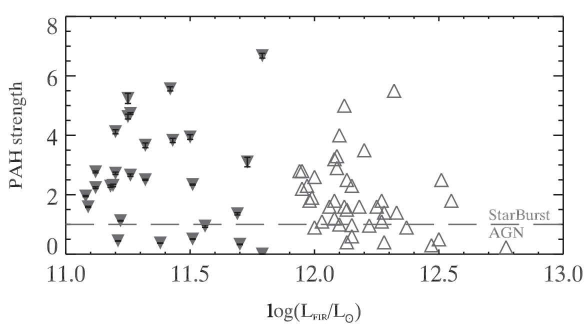

Figure 2. Comparison between the PAH 7.7 μm strengths in our LIRG sample (the filled inverted triangles) and those of the ULIRG sample of Lutz et al. (1998; the unfilled triangles), vs. the FIR luminosity for each galaxy. The dashed line is the starburst/AGN discriminator suggested by Lutz et al. (1998).

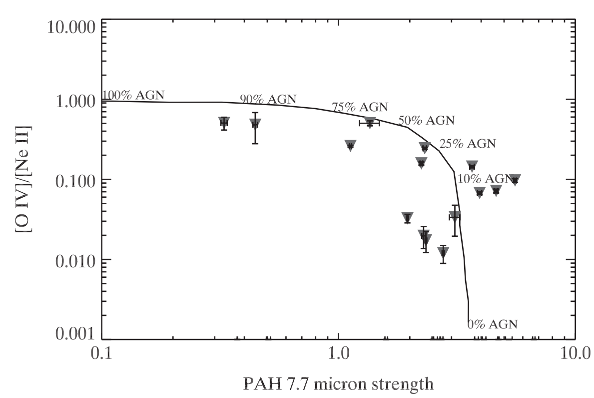

Figure 3. $\frac{[\mathrm{O\,IV}]25.9\,\mu m}{[\mathrm{Ne\,II}]12.8\,\mu m}$ ratio vs. the PAH 7.7 μm strength for each LIRG. Also shown is the Genzel et al. (1998) diagnostic curve with their percentage estimates of the AGN contribution along the curve.

4.3. $\log\left(\frac{f_{30\,\mu m}}{f_{15\,\mu m}}\right)$ Continuum Ratio

To distinguish between AGN and starburst galaxies we use the values determined by Veilleux et al. (2009) for the $\log(\frac{f_{30}}{f_{15}})$ continuum ratio and, following Veilleux et al. (2009), we interpolate between these values to give an estimate of the percentage L_{FIR} contribution from the AGN component of each galaxy (Table 3 shows the estimated AGN percentage contribution based on the $\log(\frac{f_{30}}{f_{15}})$). Six galaxies (21% of our sample) have $\log(\frac{f_{30}}{f_{15}})$ values suggesting that an AGN contributes $>$50% to their energy output.

4.4. Comparison with Existing Galaxy Classifications and Surveys

To test the assumption that AGNs have not previously been observed in the optical or near-infrared for our sample of galaxies, we searched NASA's Extragalactic Database (NED) and references therein for optical and infrared galaxy classifications of our sample. Of the 28 galaxies in our sample, 22 galaxies have classifications in NED (the NED classifications are summarized in Table 6). One galaxy (MCG +00-29-023) has been

Table 4
[Ne III]15.6 μm/[Ne II]12.8 μm and Extinction Estimates

Name	$\frac{[\text{Ne III}]15.6\,\mu\text{m}}{[\text{Ne II}]12.8\,\mu\text{m}}$ [a]	Error	% AGN[b]	$\frac{[\text{S III}]18.7\,\mu\text{m}}{[\text{S III}]33.5\,\mu\text{m}}$	Error	Relative Extinction[c] (mag)	A_v[d] (mag)
MCG−03-04-014	0.13	0.004	3	0.49	0.014	0.01	0.46
IR01364−1042	0.18	0.02	9	0.08	0.015		
NGC695	0.15	0.004	6	0.46	0.017	0.08	2.71
IR03359+1523	0.27	0.007	19	1.24	0.061		
UGC3094	0.34	0.007	27	1.13	0.042		
NGC2342	0.14	0.005	4	0.44	0.069	0.15	5.07
NGC2388	0.09	0.003	0	1.57	0.108		
MCG+08-18-012							
NGC3110	0.11	0.003	1	0.91	0.044		
IR10173−0828							
MCG−00-29-023	0.17	0.009	8	0.31	0.017	0.51	17.36
UGC6436	0.09	0.007	0	0.47	0.03	0.06	1.98
Arp193	0.16	0.002	7	0.3	0.007	0.56	18.87
MRK1490	0.09	0.004	0	1.2	0.128		
Arp302				0.97	0.224		
IZw107N	0.21	0.021	12	0.65	0.062		
NGC6090	0.24	0.004	16	0.51	0.083		
IR16164−0746		0.003		0.25	0.009	0.77	26.33
NGC6285	0.05	0.007	0	0.63	0.138		
IR17132−5313	0.21	0.005	12	0.27	0.06	0.67	22.83
IR17132−5313	0.1	0.004	0	0.36	0.01	0.34	11.67
IR17138−1017	0.16	0.004	7	0.39	0.031	0.27	9.02
Zw448.020	1.66	0.028	100	0.39	0.028	0.28	9.51
ESO602-G025	0.11	0.004	1	0.43	0.053	0.15	5.22
UGC12150	0.49	0.012	43	0.3	0.055	0.56	18.92
Zw453.062	0.06	0.007	0	0.48	0.053	0.04	1.25
MCG+07-23-019	2.73	0.04	100	0.27	0.017	0.67	22.87
cgcg052-037		0.002		0.49	0.01	0.03	1.03

Notes.
[a] [Ne III] to [Ne II] flux ratio.
[b] The estimated percentage AGN contribution to $L_{\rm FIR}$ based on linearly interpolating between 1.0 (100% AGN) and 0.1 (0% AGN).
[c] Lower limit to relative extinction estimated using the [S III]18.7 μm to [S III] 33.5 μm ratio.
[d] Lower limit to V-band extinction based on Draine (1989).

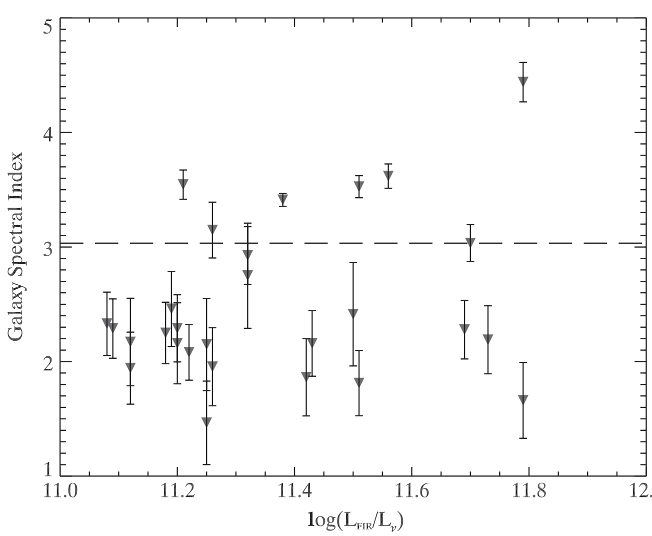

Figure 4. Spectral indices of the best-fit slope to the 7–14 μm wavelength range for each galaxy in our sample. The uncertainties are 1σ errors in the best-fit spectral indices. The dashed line shows the spectral index above which galaxies have the power-law-like spectra of AGNs and below which galaxies have starburst-like spectra.

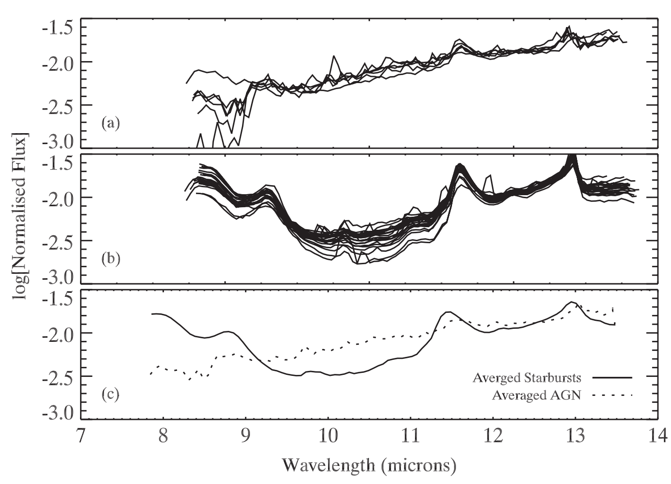

Figure 5. Panel (a) shows the normalized 7–14 μm spectra of the galaxies that are well fitted by an AGN-like power law. Panel (b) shows the normalized spectra of galaxies that have starburst-like spectra. Panel (c) shows a comparison of the average normalized spectra from panels (a) and (b).

previously classified as a Seyfert2–LINER combination. The remaining 21 galaxies are classified in NED as a combination of LINERs, LIRGs, and starburst galaxies with no evidence of AGN activity in the optical or infrared.

Table 5
The Spectral Indices for Galaxies that have AGN Power-law Shapes

Name	α	$\delta\alpha$[a]
IR03359+1523	3.41	±0.06
MCG+08-18-012	3.54	±0.13
IR10173−0828	3.03	±0.16
Arp302	3.62	±0.11
Zw448.020	4.44	±0.17
MCG+07-23-019	3.53	±0.10

Note. [a] 1σ errors in the spectral index.

Table 6
NASA Extragalactic Database Classification

Name	NED Luminosity Class/Morphology[a]	Bandpass
mcg−03-04-014	LIRG, H II	Optical; IR
IRAS 01364−1042	LINER;LIRG, H II	Optical; IR
NGC 695	S0 pec;LIRG H II	Optical; IR
IRAS 03359+1523		Optical; IR
ugc3094	LIRG; Sbc	Optical; IR
NGC 2342	S pec H II; LIRG	Optical; IR
NGC 2388	S; H II	Optical; IR
MCG +07-23-019		
NGC 3110	SB(rs)b pec;H II;LIRG	Optical; IR
IRAS 10173−0828		
MCG +08-18-012	H II	Optical
UGC 06436	SB;LINER;LIRG H II	Optical; IR
ARP193	Im: pec;H II LINER	Optical; IR
MRK 1490	Sa;LINER;LIRG H II	Optical; IR
ARP302		Optical
IZw107N		
NGC 6090	S0/Sa pair; LIRG	Optical; IR
IRAS 16164−0746	LINER; LIRG	Optical; IR
NGC 6285	S0;LINER H II	Optical
NGC 6286	Sb: pec; H II LINER; LIRG	Optical; IR
IRAS 17132−5313		
IRAS 17138−1017	S; H II	Optical; IR
ZW448.020	H I; LIRG; Pair	Optical; IR
ESO 602-G025	SA(r)b;LIRG;H II; LINER	Optical; IR
UGC 12150	SB0/a;H II:LINER	Optical; IR
ZW 453.062	LIRG; LINER	Optical; IR
MCG +00-29-023	SAB(s)b;H II Sy2	Optical; IR
CGCG 052-037	S;LINER;LIRG H II	Optical; IR

Note. [a] Uses the same notation as found in NED to describe classification.

5. EXTINCTION

We have assumed that no significant extinction correction is needed for data at these relatively long wavelengths. We justify this assumption by using the ratio [S III]18.7 μm/[S III]33.5 μm (shown in Figure 6 and in Table 4) to estimate a lower limit for extinction (Genzel et al. 1998; Verma et al. 2003). The [S III]33.5 μm line was detected in all galaxies and the [S III]18.7 μm line was detected in all but two galaxies (MCG+08-18-012, IR010173-0828), and so we have no extinction estimate for these two galaxies. The [S III] ratio is expected to have a value of ~0.5 and be insensitive to the shape of the radiation field and independent of the ionization parameter for $n_e < 10^{2.5}$ cm^{-3}. This ratio does increase with electron density and hence can provide only a lower limit to the relative extinction between these lines. Using the extinction curve of Draine (1989), and assuming the extinction at 33.5 μm is negligible, we have also estimated a lower limit for A_v (see Table 4). Figure 6 shows a plot of 0.5 times [S III]33.5 μm versus [S III]18.7 μm.

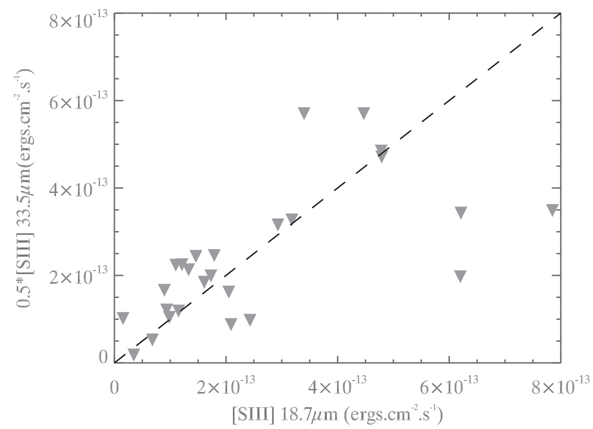

Figure 6. 0.5 times the flux of [S III]33.5 μm vs. the flux of [S III]18.7 μm. The dashed line is the line of zero relative extinction and galaxies suffering from extinction will fall below this line.

The dashed line on this figure is the line of zero relative extinction between the two [S III] lines. Galaxies suffering high extinction will fall below this line. For all other galaxies the relative extinctions calculated from the [S III] ratio are small and the spread of data points around the zero extinction line is primarily due to the uncertainty in the line flux measurements.

6. DISCUSSION

The present sample of 28 LIRGs was selected from a larger sample of 47 LIRGs (43 systems) observed by Goldader et al. (1997). This sample of 28 LIRGs included only LIRGs that showed no indications of AGNs in the optical or near-infrared. This looked to be strong evidence that there were no AGNs buried in dust, since the extinction at 2.2 μm is about ten times less than that in the visible. Moreover, the 2.2 μm spectroscopic diagnostics indicate that the infrared luminosities could be completely understood in terms of a recent burst of star formation.

How does this conclusion change in view of the *Spitzer* mid-infrared spectroscopy reported here? First, we can confirm that these galaxies *all* have significant ongoing star formation. The estimated star formation rate for each galaxy can be found in Table 3. These estimates were produced using the calibration of Ho & Keto (2007) to convert ($L_{[\mathrm{Ne\,II}]}+L_{[\mathrm{Ne\,III}]}$) to a star formation rate. The average star formation rate is about 50 solar masses per year, and the total star formation rate accounts for ~(80 ± 4)% of the L_{FIR} of the LIRG sample.

Second, and perhaps more surprisingly, one or more mid-infrared lines which are almost certainly due to AGNs, [Ne V]14.3 μm, [Ne V]24.3 μm, or strong [O IV]25.9 μm, are detected in nearly half the sample, as may be seen in Table 3. Consequently, there is conclusive evidence for the co-existence of AGNs and starbursts in half of this sample, none of which showed any evidence for AGNs in optical or near-infrared spectroscopy. And so a second conclusion from this study is that LIRGs—even those selected as having no evidence for AGNs at wavelengths as long as 2 μm—frequently exhibit the presence of both AGNs and starbursts, if one observes them at longer infrared wavelengths less affected by extinction. This provides further evidence complementing the studies referred to in the Introduction that find starbursts associated with AGNs. In this case it is AGNs that are found in a sample of classic LIRGs that had been previously classified as starbursts. And while a correlation does not prove there is a causal

Table 7
Results Summary

Name	$\frac{[\mathrm{Ne\,V}]14.3\,\mu\mathrm{m}}{[\mathrm{Ne\,II}]12.8\,\mu\mathrm{m}}$ [a]	$\frac{[\mathrm{Ne\,V}]24.3\,\mu\mathrm{m}}{[\mathrm{Ne\,II}]12.8\,\mu\mathrm{m}}$	$\frac{[\mathrm{O\,IV}]25.9\,\mu\mathrm{m}}{[\mathrm{Ne\,II}]12.8\,\mu\mathrm{m}}$	$\frac{[\mathrm{Ne\,III}]15.6\,\mu\mathrm{m}}{[\mathrm{Ne\,II}]12.8\,\mu\mathrm{m}}$ [b]	PAH 7.7 μm Strength[c]	$\log(\frac{f_{30\,\mu\mathrm{m}}}{f_{15\,\mu\mathrm{m}}})$[d]	Power-law Continuum[e]
MCG−03-04-014		SB-AGN	SB-AGN				
IR01364−1042			AGN		AGN		
NGC695					SB-AGN	AGN	
IR03359+1523					AGN	AGN	AGN
UGC3094			AGN		AGN	AGN	
NGC2342					SB-AGN		
NGC2388							
MCG+08-18-012			AGN		AGN	AGN	AGN
NGC3110							
IR10173−0828		AGN	AGN		AGN		AGN
MCG−00-29-023					AGN		
UGC6436							
Arp193							
MRK1490							
Arp302					AGN	AGN	AGN
IZw107N							
NGC6090					SB-AGN		
IR16164−0746							
NGC6285							
IR17132−5313			SB-AGN				
IR17132−5313							
IR17138−1017							
Zw448.020	AGN	SB-AGN		AGN	AGN	AGN	AGN
ESO602-G025					SB-AGN		
UGC12150							
Zw453.062	SB-AGN	SB-AGN	AGN				
MCG+07-23-019	AGN			AGN	AGN		AGN
cgcg052-037							

Notes.
[a] Line ratios [Ne v]14.3 μm/[Ne ii]12.8 μm, [Ne v]24.3 μm/[Ne ii]12.8 μm, and [O iv]25.9 μm/[Ne ii]12.8 μm above 50% of level for the AGNs of Sturm et al. (2002) $\Longrightarrow$ AGN (significant AGN contribution) and line ratios above 25% of level for the AGNs of Sturm et al. (2002) $\Longrightarrow$ SB-AGN (some AGN contribution but AGN is not dominant).
[b] The AGNs in Sturm et al. (2002) have a median [Ne iii]15.6 μm/[Ne ii]12.8 μm of 1.1, and their starburst templates have a median value of 0.1. A value above 1.1 for this line ratio $\Longrightarrow$ AGN (significant AGN contribution), and a line ratio of 0.35 (linearly interpolated to 25% of the AGN ratio) $\Longrightarrow$ SB-AGN (some AGN contribution but AGN is not dominant).
[c] Genzel et al. (1998) template starbursts have average PAH strengths of 3.1 and their AGN templates have average PAH strengths of 2.1, with a standard deviation of about 1.0 in each case. We assume a PAH strength of 1.0 is ∼100% AGN-dominated and linearly interpolate between 3.1 and 1.0 to estimate an approximate precentage contribution. Galaxies with PAH-derived AGN contributions above 50% $\Longrightarrow$ AGN (significant AGN contribution). Galaxies with PAH-derived AGN contributions above 25% $\Longrightarrow$ SB-AGN (some AGN contribution but AGN is not dominant).
[d] The linear calibration of Veilleux et al. (2009) is assumed to drive approximate AGN contributions. Galaxies with $\log(\frac{f_{30}}{f_{15}})$ AGN contributions above 50% of this linear calibration $\Longrightarrow$ AGN (significant AGN contribution).
[e] Galaxies with continua that are well fitted by power law $\Longrightarrow$ AGN.

connection, these results do suggest that processes which stimulate starbursts also may result in triggering the onset of AGNs, as suggested in the modeling of Hopkins et al. (2010) and others.

Third, what does one learn about the relative dominance of starbursts or AGNs in producing the large infrared luminosities of these galaxies? Seven galaxies (25% of the sample) have significant AGN signatures for at least three of the seven basic diagnostics used to detect AGNs. Table 7 shows a summary of the results of applying each diagnostic. The median percentage of AGN detections by all seven diagnostics is 18%. In addition, using the Genzel et al. (1998) diagnostic curve to estimate the contribution of AGNs we find three galaxies (11% of the sample, IR01364−1042, MCG+08-18-012, IR10173−0828) in which AGNs contribute more than 50% of the L_{FIR}. Consequently, the luminosities of these three galaxies are probably dominated by the output of their AGNs. Also using the Genzel et al. (1998) curve, we find that a further 12 galaxies (43% of the sample, mcg-03-04-014, NGC695, ugc3094, NGC2342, NGC2388, NGC3110, ARP193, IZw107N, IR16164−0746, NGC 6286, ESO 602-G025, ZW 453.062) have AGNs that contribute between 5% and 50% of the galaxy's luminosity. Counting the total contribution of AGNs given by the Genzel et al. (1998) curve we find that ∼(17 ± 4)% of the total L_{FIR} of the sample is produced by AGNs. Additionally, using linear interpolation, the basic diagnostics suggest the following estimated AGN contributions to the total L_{FIR} of the sample: $\frac{[\mathrm{Ne\,V}]14.3\,\mu\mathrm{m}}{[\mathrm{Ne\,II}]12.8\,\mu\mathrm{m}} = 16\%$, $\frac{[\mathrm{Ne\,V}]24.3\,\mu\mathrm{m}}{[\mathrm{Ne\,II}]12.8\,\mu\mathrm{m}} = 15\%$, $\frac{[\mathrm{O\,IV}]25.9\,\mu\mathrm{m}}{[\mathrm{Ne\,II}]12.8\,\mu\mathrm{m}} = 11\%$, $\frac{[\mathrm{Ne\,III}]15.6\,\mu\mathrm{m}}{[\mathrm{Ne\,II}]12.8\,\mu\mathrm{m}} = 18\%$, $\log(\frac{f_{30}}{f_{15}}) = 44\%$, and PAH 7.7 μm $= 38\%$. These give a median value for the AGN contribution from the basic diagnostics of 17%. The wide variation in the contribution estimates for the simple diagnostics is in part due to the roughness of linearly interpolating between AGN and starburst values and in part due to the fact that real AGNs and starbursts have values that are scattered around the assumed AGN and starburst values that were used as the end points for each interpolation.

Previous studies of ULIRGs (Genzel et al. 1998; Lutz et al. 1998; Armus et al. 2007; Farrah et al. 2007) have found 20%–30% of ULIRGs have luminosities dominated by an AGN. More recent multiwavelength observations of both LIRGs and ULIRGs by Kartaltepe et al. (2010) found that about 10% of LIRGs and about 40% of ULIRGs were likely to be dominated by the luminosity of an AGN. While these are somewhat rough numbers, they do suggest that a slightly higher fraction of ULIRGs may be dominated by an AGN compared to those of LIRGs.

A recent paper by Petric et al. (2011) provides a statistical analysis of the *Spitzer* spectra for 248 LIRGs. Spectra for individual galaxies are not given, but since the data have been taken from the *Spitzer* archive, it will include the data for the 28 LIRGs presented herein. Petric et al. (2011) find a median AGN contribution of 12% to the luminosity of local LIRGs, which is consistent with the 17% found for our LIRG sample.

7. SUMMARY AND CONCLUSIONS

Mid-infrared spectroscopy has been obtained for a sample of 28 LIRGs, none of which showed evidence of AGNs in the optical or in 2.2 μm infrared spectroscopy. Seven basic diagnostics were applied to search for AGNs in these galaxies (the results of which are summarized in Table 7). Two of these diagnostics (the [O IV]25.9 μm/[Ne II]12.8 μm and the PAH 7.7 μm strength) were used with the Genzel et al. (1998) calibration curve to estimate the contribution of AGNs to each galaxy's far-infrared luminosity. Additionally, the ($L_{[\mathrm{Ne\,II}]}$ + $L_{[\mathrm{Ne\,III}]}$) was used to estimate the star formation rate of each galaxy. Our results lead to the following conclusions.

1. There is active star formation present in the entire sample.
2. The average estimated star formation rate per galaxy is 50 solar masses per year and the total star formation accounts for about (80 $\pm$ 4)% of the total FIR luminosity.
3. The median fraction of AGN detections for all seven simple diagnostics is 18% and there are 11 galaxies (39% of the sample) in which at least two of the seven simple diagnostics suggest the presence of an AGN. These diagnostics indicate that there may be AGNs in $\sim$57% of our LIRG sample. Using the Genzel et al. (1998) diagnostic, we found 3 galaxies (11% of the sample) that may be dominated by AGNs and a further 12 galaxies (43% of the sample) that have between 5% and 50% of their luminosity provided by AGNs. The Genzel et al. (1998) diagnostic curve thus indicates that $\sim$54% of our LIRG sample may have AGNs.
4. Using the diagnostic curve of Genzel et al. (1998) we estimated that AGNs contribute $\sim$(17 $\pm$ 4)% of the total L_{FIR} of the sample. Using the basic diagnostics $\frac{[\mathrm{Ne\,V}]14.3\,\mu\mathrm{m}}{[\mathrm{Ne\,II}]12.8\,\mu\mathrm{m}}$, $\frac{[\mathrm{Ne\,V}]24.3\,\mu\mathrm{m}}{[\mathrm{Ne\,II}]12.8\,\mu\mathrm{m}}$, $\frac{[\mathrm{O\,IV}]25.9\,\mu\mathrm{m}}{[\mathrm{Ne\,II}]12.8\,\mu\mathrm{m}}$, $\frac{[\mathrm{Ne\,III}]15.6\,\mu\mathrm{m}}{[\mathrm{Ne\,II}]12.8\,\mu\mathrm{m}}$, $\log(\frac{f_{30}}{f_{15}})$, and PAH 7.7 μm and linearly interpolating between AGN and starburst values we estimated that AGNs contribute 17% of the sample's L_{FIR}.
5. Spectroscopy at wavelengths in the optical or near-infrared is likely to miss an AGN buried in extinction in these dusty infrared-bright galaxies.

This work is based (in part) on observations made with the *Spitzer Space Telescope*, which is operated by the Jet Propulsion Laboratory, California Institute of Technology under a contract with NASA. Support for this work was provided by NASA through an award issued by JPL/Caltech.

This research has made use of the NASA/IPAC Extragalactic Database (NED) which is operated by the Jet Propulsion Laboratory, California Institute of Technology, under contract with the National Aeronautics and Space Administration.

REFERENCES

Armus, L., Charmandaris, V., Bernard-Salas, J., et al. 2007, ApJ, 656, 148
Barnes, J. E., & Hernquist, L. 1992, ARA&A, 30, 705
Barnes, J. E., & Hernquist, L. E. 1991, ApJ, 370, L65
Brandl, B. R., Bernard-Salas, J., Spoon, H. W. W., et al. 2006, ApJ, 653, 1129
Cid Fernandes, R., Heckman, T., Schmitt, H., González Delgado, R. M., & Storchi-Bergmann, T. 2001, ApJ, 558, 81
Draine, B. T. 1989, in Infrared Spectroscopy in Astronomy, ed. B. H. Kaldeich (ESA SP-290; Noordwijk: ESA), 93
Farrah, D., Bernard-Salas, J., Spoon, H. W. W., et al. 2007, ApJ, 667, 149
Genzel, R., Lutz, D., Sturm, E., et al. 1998, ApJ, 498, 579
Goldader, J. D., Joseph, R. D., Doyon, R., & Sanders, D. B. 1997, ApJS, 108, 449
Heckman, T. M., van Breugel, W., Miley, G. K., & Butcher, H. R. 1983, AJ, 88, 1077
Ho, L. C., & Keto, E. 2007, ApJ, 658, 314
Hopkins, P. F., Younger, J. D., Hayward, C. C., Narayanan, D., & Hernquist, L. 2010, MNRAS, 402, 1693
Houck, J. R., Roellig, T. L., van Cleve, J., et al. 2004, ApJS, 154, 18
Joseph, R. D. 1999, Ap&SS, 266, 321
Joseph, R. D., Meikle, W. P. S., Robertson, N. A., & Wright, G. S. 1984, MNRAS, 209, 111
Joseph, R. D., & Wright, G. S. 1985, MNRAS, 214, 87
Kartaltepe, J. S., Sanders, D. B., Le Floc'h, E., et al. 2010, ApJ, 709, 572
Larson, R. B., & Tinsley, B. M. 1978, ApJ, 219, 46
Laurent, O., Mirabel, I. F., Charmandaris, V., et al. 2000, A&A, 359, 887
Lutz, D., Spoon, H. W. W., Rigopoulou, D., Moorwood, A. F. M., & Genzel, R. 1998, ApJ, 505, L103
Mihos, J. C., & Hernquist, L. 1996, ApJ, 464, 641
Noguchi, M. 1988, A&A, 203, 259
Peeters, E., Spoon, H. W. W., & Tielens, A. G. G. M. 2004, ApJ, 613, 986
Petric, A. O., Armus, L., Howell, J., et al. 2011, ApJ, 730, 28
Rieke, G. H., & Low, F. J. 1972, ApJ, 176, L95
Roche, P. F., Aitken, D. K., & Smith, C. H. 1991, MNRAS, 252, 282
Rodriguez Espinosa, J. M., Rudy, R. J., & Jones, B. 1987, ApJ, 312, 555
Sanders, D. B. 1999, Ap&SS, 266, 331
Sani, E., Lutz, D., Risaliti, G., et al. 2010, MNRAS, 403, 1246
Schweizer, F. 2005, in Starbursts: From 30 Doradus to Lyman Break Galaxies, ed. R. de Grijs & R. M. González Delgado (Astrophysics and Space Science Library, Vol. 329; Dordrecht: Springer), 143
Shier, L. M., Rieke, M. J., & Rieke, G. H. 1996, ApJ, 470, 222
Soifer, B. T., Sanders, D. B., Madore, B. F., et al. 1987, ApJ, 320, 238
Spinoglio, L., & Malkan, M. A. 1992, ApJ, 399, 504
Storchi-Bergmann, T., González Delgado, R. M., Schmitt, H. R., Cid Fernandes, R., & Heckman, T. 2001, ApJ, 559, 147
Sturm, E., Lutz, D., Verma, A., et al. 2002, A&A, 393, 821
Tielens, A. G. G. M., Peeters, E., Bakes, E. L. O., Spoon, H. W. W., & Hony, S. 2004, in ASP Conf. Ser. 323, Star Formation in the Interstellar Medium: In Honor of David Hollenbach, ed. D. Johnstone, F. C. Adams, D. N. C. Lin, D. A. Neufeeld, & E. C. Ostriker (San Francisco, CA: ASP), 135
Toomre, A., & Toomre, J. 1972, ApJ, 178, 623
Veilleux, S., Rupke, D. S. N., Kim, D.-C., et al. 2009, ApJS, 182, 628
Verma, A., Lutz, D., Sturm, E., et al. 2003, A&A, 403, 829
Weedman, D. W., Hao, L., Higdon, S. J. U., et al. 2005, ApJ, 633, 706
Werner, M. W., Roellig, T. L., Low, F. J., et al. 2004, ApJS, 154, 1
Wright, G. S., Joseph, R. D., Robertson, N. A., James, P. A., & Meikle, W. P. S. 1988, MNRAS, 233, 1